Molecular Therapy
Oncolytics
Original Article

Development of a seven-gene tumor immune microenvironment prognostic signature for high-risk grade III endometrial cancer

Mingjun Zheng,[1,2,3] Yuexin Hu,[1,2] Rui Gou,[1,2] Siting Li,[1,2] Xin Nie,[1,2] Xiao Li,[1,2] and Bei Lin[1,2]

[1]Department of Gynecology and Obstetrics, Shengjing Hospital of China Medical University, Liaoning 110004, China; [2]Key Laboratory of Maternal-Fetal Medicine of Liaoning Province, Key Laboratory of Obstetrics and Gynecology of Higher Education of Liaoning Province, China; [3]Department of Obstetrics and Gynecology, University Hospital, LMU Munich, Maistrasse 11, 80337 Munich, Germany

Uterine corpus endometrial carcinoma locally infiltrates numerous immune cells and other tumor immune microenvironment components. These cells are involved in malignant tumor growth and proliferation and the process of resistance toward immunotherapies. Here, we aimed to develop a tumor immune microenvironment-related prognostic signature for high-risk grade III endometrial carcinoma based on The Cancer Genome Atlas. The signature was systematically correlated with immune infiltration characteristics of the tumor microenvironment. The seven-gene Riskscore signature was robust and performed well in training, testing, and Gene Expression Omnibus-independent cohorts. A nomogram comprising the gene signature accurately predicted patient prognosis, with our model performing better than other endometrial cancer-related signatures. Analysis of the IMvigor210 immunotherapy cohort revealed that subgroups with a low Riskscore had a better prognosis than subgroups with a high Riskscore. Subgroups with a low Riskscore exhibited immune cell infiltration and inflammatory profiles, whereas subgroups with a high Riskscore experienced progressive disease. The receiver operating characteristic curve indicated that risk score, neoantigen, and tumor mutation burden models together accurately predicted treatment response. Taken together, we developed a tumor microenvironment-based seven-gene prognostic stratification system to predict the prognosis of patients with high-risk endometrial cancer and guide more effective immunotherapy strategies.

INTRODUCTION

Uterine corpus endometrial carcinoma (UCEC) is one of the three most common gynecological malignancies and the fourth most common cancer type affecting women in developing countries.[1] In 2015, the number of new endometrial cancer cases in China was expected to be 63,400, with an estimated death toll of 21,800.[2] Approximately three- quarters of the patients with UCEC are diagnosed early, with a 5-year survival rate of more than 70%.[3–5] However, the prognosis of patients with high-risk UCEC, including FIGO (International Federation of Gynecology and Obstetrics) grade III endometrioid cancer, clear cell carcinoma, serous carcinoma, and mixed adenocarcinoma, is still poor in addition to the risk of metastasis and recurrence being very high. The 5-year survival rate is only 17%.[6–9]

The tumor microenvironment (TME) is comprised of tumor cells, stromal cells, endothelial cells, immune cells, and extracellular matrix secreted by tumor-associated cells. TME components interact with tumor cells to regulate their growth and development.[10]

In recent years, increasing evidence has shown that the occurrence, development, and metastasis of malignant tumor cells are all related to the TME.[11–13] The tumor immune microenvironment (TIME), as part of the TME, plays an important role in tumor progression.[14] In addition, it suppresses immune cells, allowing for immune evasion and tolerance of tumor cells, which in turn affects tumor occurrence and progression. Given the abundance of immune cells and cytokines found in UCEC,[15] it can be inferred that the TME plays a major role in UCEC development and immunotherapy response.

In this genomic era, a large number of genome-sequencing technologies and data have emerged,[16] and researchers began to focus on the prognosis prediction of UCEC using The Cancer Genome Atlas (TCGA)-UCEC cohort.[17–20] Wang et al.[17] constructed an autophagy-related long-noncoding RNA signature to predict the prognosis of UCEC. Jiang et al.[18] and Liu et al.[19] constructed a glycolysis-related gene signature to predict the prognosis of UCEC. However, these studies are limited to the analysis of specific genes and prognosis in all TCGA-UCEC samples and lack external verification. Therefore, the prediction of the prognosis of high-risk UCEC accurately remains a challenge.

In this study, we included all high-risk grade III tumor samples in TCGA-UCEC, comprising mixed-type, serous, and endometrioid

Received 17 February 2021; accepted 2 July 2021;
https://doi.org/10.1016/j.omto.2021.07.002.

Correspondence: Bei Lin, 4th Gynecological Ward, Department of Gynecology and Obstetrics, Shengjing Hospital of China Medical University, 36 Sanhao Street, Shenyang, Liaoning 110004, China.
E-mail: linbei88@hotmail.com

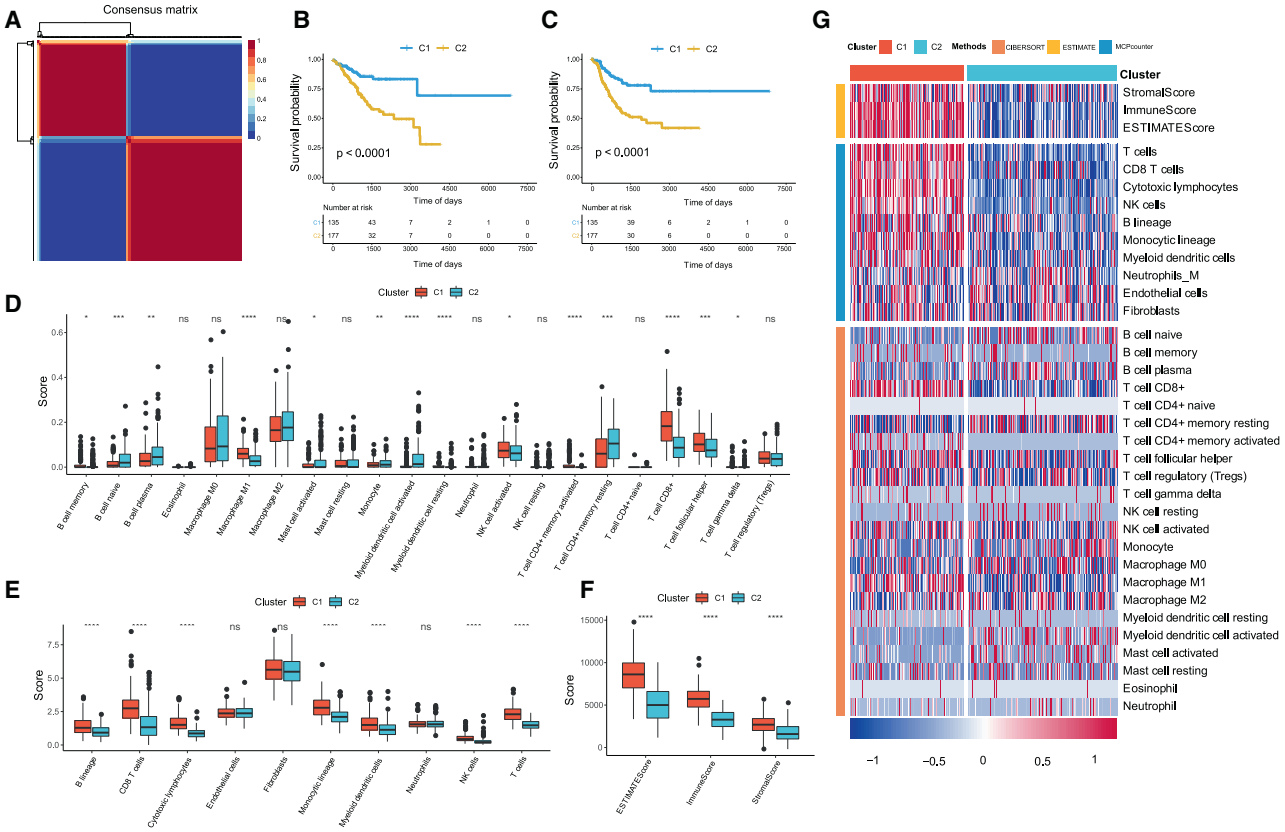

Figure 1. Identification of molecular subtype based on TIME genes

(A) NMF cluster consensus map. (B) OS curve of UCEC molecular subtypes. (C) PFS curve of UCEC molecular subtypes. (D) Comparison of molecular subtypes based on 22 immune cell types. (E) Comparison of MCPcounter immune scores among molecular subtypes. (F) Comparison of ESTIMATE immune scores among molecular subtypes. (G) Heatmap for the comparison of three immune scores among molecular subtypes.

endometrial adenocarcinoma (SEA and EEA, respectively). Then, an immune prognostic signature of grade III UCEC was constructed based on TIME genes and validated in different cohorts. In addition, we evaluated the prognostic merit of the seven-gene signature for immunotherapy response. The current findings revealed that the gene signature could be used to evaluate the prognosis of patients with grade III UCEC and guide clinical decision-making, including immunotherapy-related choices.

RESULTS

Identification of two molecular subtypes based on TIME genes

After deduplication and filtering, the expression profile of 1,356 tumor immune-related genes in TCGA was extracted and analyzed by univariate Cox analysis (Table S1), and 195 genes related to the prognosis of UCEC were obtained (Table S2; $p < 0.05$). Non-negative matrix factorization (NMF) helps extract the biological correlation coefficients of the data in the gene expression matrix and obtain the internal characteristic structure of the data and finally groups the samples. This approach is widely used in the molecular classification of cancers at present. With the use of the NMF algorithm, the optimal number of subtypes was two (Figures 1A, S1A, and S1B). The C2 subtype has a significantly worse prognosis than C1 in terms of overall survival (OS) and progression-free survival (PFS) (Figures 1B and 1C; log-rank $p < 0.01$). The R software package ESTIMATE was used to evaluate StromalScore, ImmuneScore, and ESTIMATEScore between C1 and C2 subtypes. Further, MCPcounter was used to evaluate 10 immune cell types, and CIBERSORT was employed to evaluate 22 immune cell types. ESTIMATE and MCPcounter results revealed that the tumor immune infiltration degree of the C1 subtype was mostly higher than that of the C2 subtype (Figures 1E and 1F). CIBERSORT results indicated that M1 macrophages, $CD8^+$ T cells, and follicular helper T cell abundance in the C1 subtype were significantly higher than in the C2 subtype (Figure 1D). Furthermore, the distribution of tumor-infiltrating immune cells (TIICs) between the two subtypes, as evaluated by the three methods, was nearly the same. We, therefore, speculated that the C1 subtype may have a better response to immunotherapy. The heatmap of TIIC distribution for the two subtypes is shown in Figure 1G.

Further, we compared the distribution of histopathological subtypes' age, FIGO stage, and survival between the two molecular subtypes. The results showed that the C1 subtype is dominated by EEA samples,

Table 1. TCGA training set and validation set sample information

Clinical features	TCGA-UCEC train	TCGA-UCEC test	p
OS			
0	119	124	0.5853
1	37	32	
Stage			
I	81	84	0.6354
II	19	15	
III	46	42	
IV	10	15	
Age			
≤65	75	78	0.9436
>65	80	77	
Unknown	1	1	

whereas in the C2 subtype, most samples are SEA (Figure S1C). The survival rates for the two subtypes were significantly different, with the mortality rate of the C2 subtype being higher (Figure S1D). The age ratios of the two subtypes were significantly different, as the proportion of middle-aged patients in subtype C2 was higher (Figure S1E). There was also a significant difference in the proportion of FIGO stages between the two subtypes, as the proportion of patients with FIGO stage II, III, and IV was higher in the C2 subtype than in the C1 subtype (Figure S1F).

Identification of differentially expressed genes (DEGs) between subtypes

As previously described, we obtained 883 DEGs (Table S3), and the volcano map of upregulated and downregulated DEGs between the C1 and C2 subtypes is shown in Figure S1G. Among them, 443 genes were upregulated, whereas 440 genes were downregulated. We selected the top 100 genes with the most significant upregulation or downregulation to construct a heatmap, which is shown in Figure S1H. DEGs between C1 and C2 have evident distribution characteristics.

Construction of a prognostic multi-gene signature based on TIME subtype

TCGA cohort was divided into training and testing cohorts, with 156 samples each (Table 1). Based on the training cohort, the univariate Cox proportional hazard regression model was employed to identify prognostic DEGs between the subtypes with the threshold value of $p < 0.05$. Finally, 42 prognostic hub genes were obtained (Table S4). These genes may serve as potential TIME-related characteristic genes.

As an excessively large number of genes are not conducive to clinical detection, we further narrowed the range of immune-related genes. We employed the least absolute shrinkage and selection operator (Lasso) regression analysis, and the resulting change trajectory of each independent variable is shown in Figure 2A. With the gradual increase of lambda, the number of independent variable coefficients gradually increased to zero. Five-fold cross-validation was used to build the model, and the confidence interval under each lambda is shown in Figure 2B, indicating that when log(lambda) = −3.65, the model was optimal. Thus, we selected 18 genes at lambda = 0. 0262 as the candidate genes. As described in Materials and methods, in order to obtain the best fit of the model, the Akaike information criterion (AIC) method was then employed from which we obtained seven genes, namely DRAM1, TNFRSF14, SCGB2A1, EMX2, DNER, DAPL1, and interferon-induced protein with tetratricopeptide repeats sequence 1 (IFIT1). The seven-gene signature estimated Riskscore (RS) is as follows: RS = −0.621 · DRAM1 − 0.343 · tumor necrosis factor receptor (TNFR)SF14 − 0.106 · SCGB2A1 − 0.433 · EMX2 + 0.259 · DNER + 0.248 · DAPL1 + 0.344 · IFIT1.

To obtain a fixed grouping threshold between different cohorts, we converted RS to standard score; the samples with RS greater than zero are divided into high-risk groups (HRGs), whereas those with less than zero are divided into low-risk groups (LRGs). The Kaplan-Meier (KM) curve is shown in Figure 2C. Seventy-one samples were added into the HRG and 85 samples into the LRG. There was a significant difference in survival between the HRG and LRG ($p < 0.0001$). R software package timeROC was used to analyze the prognostic efficiency of the RS. The area under the curves (AUCs) of gene signature for 1-year, 3-year, and 5-year survival were 0.79, 0.82, and 0.89, respectively (Figure 2D).

Internal and external validation of the robustness of the signature

To determine the robustness of the signature, internal cohorts (TCGA testing and TCGA-UCEC), along with an external cohort, named Gene Expression Omnibus (GEO): GSE119041, were used for validation. The RS was calculated using the same formula as the training cohort. Subsequently, the samples are divided into HRG and LRG according to the previous step.

Significant prognostic differences were observed between the HRG and LRG from TCGA testing cohort (Figure 3A; $p < 0.01$). The AUCs of 1-year, 3-year, and 5-year survival in TCGA testing cohort were 0.62, 0.71, and 0.69, respectively (Figure 3B).

In the entire TCGA-UCEC cohort, significant prognostic differences were also observed between the HRG and LRG (Figure 3C; $p < 0.01$). The AUCs of 1-year, 3-year, and 5-year survival in TCGA-UCEC cohort were 0.72, 0.77, and 0.80, respectively (Figure 3D).

In the GEO: GSE119041 cohort, the prognosis of the HRG was significantly worse than that of the LRG (Figure 3E; $p < 0.05$). Lastly, the AUCs of 1-year, 3-year, and 5-year survival in the GEO: GSE119041 cohort were 0.76, 0.79, and 0.78, respectively (Figure 3F). These results indicated that our model performed robustly in different cohorts.

Performance of RS with regard to clinical features

The RS constructed by the seven-gene signature could effectively distinguish between the HRG and LRG with regard to age and

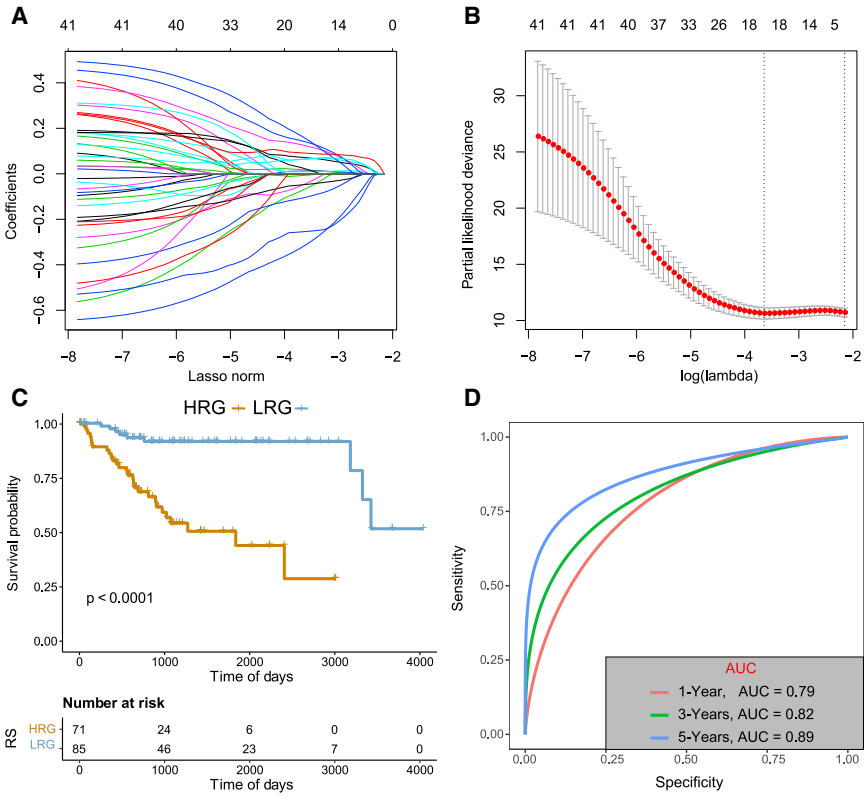

Figure 2. Analysis of Lasso regression

(A) The changing trajectory of each independent variable (the abscissa represents the corrected lambda, and the ordinate represents the coefficient of the independent variable). (B) The log value of the independent variable lambda (the abscissa represents the confidence interval of each lambda, and the ordinate represents errors in cross validation). (C) The KM curve of the seven-gene signature-based stratification in TCGA training cohort. (D) The 1-, 3-, and 5-year ROC curve based on seven-gene signature stratification.

FIGO stage (Figures 4A–4D; $p < 0.05$). The RS of the group over 65 years old was higher than that of the group ≤65 years old (Figure 4E). In addition, the advanced FIGO stage had a higher RS than the early stage (Figure 4F). Between the molecular subtypes, the RS of the poor prognosis C2 subtype was higher than the C1 subtype (Figure 4G). These findings indicated that our signature had a good ability to predict prognosis based on different clinical characteristics.

We further explored the relevant pathways that characterize the different clinical features of RS. R software package gene set variation analysis (GSVA) was used to perform gene set enrichment analysis (GSEA) for each sample, then calculated the correlation between biological pathways and the RS, and selected the top 22 pathways with a correlation greater than 0.3 for visual display (Figure 4H). It is evident that INTESTINAL_IMMUNE_NETWORK_FOR_IGA_PRODUCTION, T_CELL_RECEPTOR_SIGNALING_PATHWAY, and NATURAL_KILLER_CELL_MEDIATED_CYTOTOXICITY tumor immune-related pathways are negatively correlated with RS (Figure 4I).

Construction and evaluation of nomograms comprising the signature

The independence of the seven-gene signature in clinical application was evaluated by univariate and multivariate Cox regression analyses. The results revealed that RS was significantly correlated with prognosis in both the univariate model (hazard ratio [HR] = 3.80, $p < 0.001$) and multivariate model (HR = 3.60, $p < 0.001$) (Figures 5A and 5B), indicating that the seven-gene signature had a good clinical predictive value.

Based on the results of multivariate Cox analysis, significant clinical features such as FIGO stage and RS were combined to construct a nomogram (Figure 5C). The nomogram comprising the RS and FIGO stage proved useful to predict survival.

Calibration curves were used to visualize the performance of 1-, 3-, and 5-year nomograms. In each case, the 45° line represents the best predictive ability. The calibration results indicated that the nomogram performed well (Figure 5D). The AUC of the 1-, 3-, and 5-year nomograms was larger than that of the other clinical variables (Figures 5E–5G). Decision curve analysis (DCA) was used to assess the validity of the signature, and the nomogram showed the greatest net benefit (Figures 5H–5J). These results suggested that the nomogram is better for predicting the survival of patients with grade III UCEC than using a single clinical factor. Thus, it may be useful during the clinical decision-making process and for choosing individualized treatments.

The seven-gene signature performed better than others in prognostic prediction

To determine whether our seven-gene signature had a superior predictive ability for TCGA-UCEC cohort, we compared it with four published prognostic signatures, namely, a nine-gene signature (Jiang et al.[21]), a seven-gene signature (Liu et al.[22]), a six-gene signature (Wang et al.[23]), and another nine-gene signature (O'Mara et al.[24]). To make signatures comparable, we calculated the RS of each UCEC sample in all TCGA cohorts by the same method and converted the RS according to the previous methods in the four signatures. All four signatures could effectively divide patients into two subgroups with significantly different prognoses (Figures 6A–6C and 6G). However, receiver operating characteristic (ROC) analysis revealed that the AUC values of the four signatures for 1-, 3-, and 5-year survival were lower than those of our model (Figures 6D–6F, and 6H). The restricted mean survival (RMS)

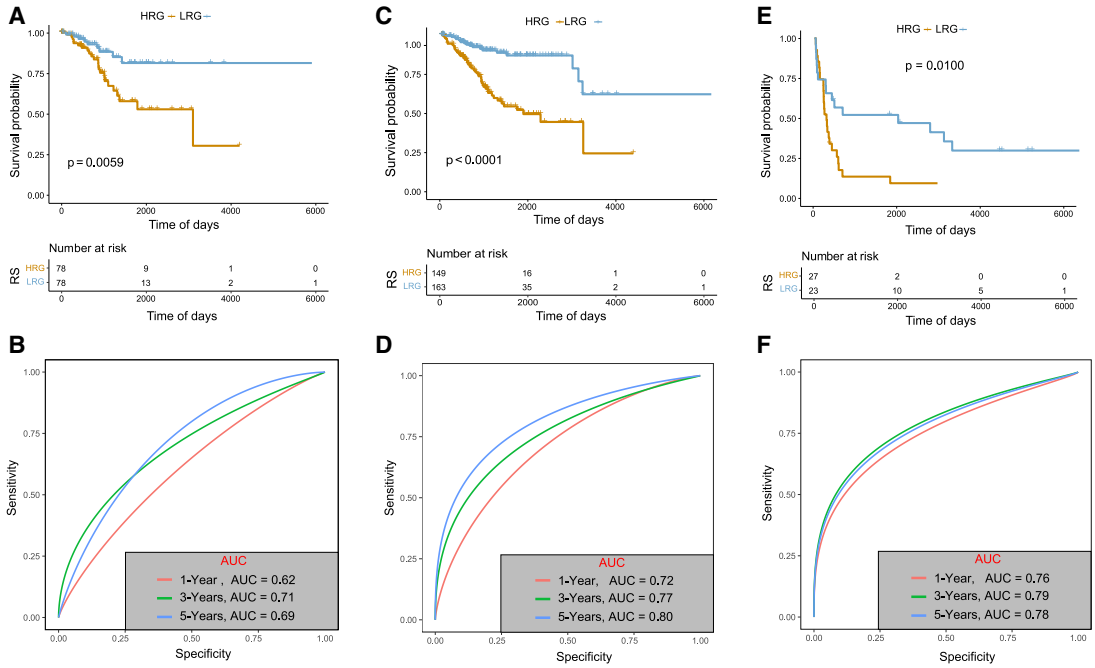

Figure 3. Validation of the seven-gene prognostic signature

(A) The OS curve of seven-gene signature classification in TCGA testing cohort. (B) The 1-, 3-, and 5-year ROC curve based on seven-gene signature stratification. (C and D) The OS curve of seven-gene signature-based stratification and 1-, 3-, and 5-year ROC curve of TCGA-UCEC cohort. (E and F) The OS curve of the seven-gene signature-based stratification and the 1-, 3-, and 5-year ROC curve in the GEO: GSE119041 cohort.

package was used to calculate the C-index of all prognostic signatures. Our model had the highest C-index at 0.72 (Figure 6I). These findings highlighted the superior predictive performance of our TIME gene signature.

The seven-gene signature effectively predicted the efficacy of immunotherapy

The identification of novel predictive markers is essential for effective immunotherapy. We obtained an immunotherapy cohort (IMvigor210) to explore whether the seven-gene signature could predict the benefit of immunotherapy.[25] The IMvigor210 cohort contains a gene expression profile for patients with or without beneficial responses to anti-programmed death ligand 1 (PD-L1) immunotherapy for metastatic urothelial carcinoma (MUC). The KM curve indicated that the prognosis of HRG was worse than that of patients with LRG (Figure 7A). The ROC curve indicated that the combination of the RS, neoantigen (NEO), and tumor mutational burden (TMB) models with logistic regression could predict treatment response with 83% accuracy, which was higher than that of NEO (AUC = 0.62) or TMB (AUC = 0.56) alone (Figure 7B). MCPcounter was used to calculate the immune cell scores of IMvigor210 samples. The results revealed that RS was negatively correlated with TMB and NEO, as well as T, natural killer (NK), and B cell scores (Figure 7C).

The violin map further indicated that the RS was significantly higher for patients with stable diseases (SD) or progressive diseases (PD) than for those with complete responses (CR) or a partial response (PR) (Figure 7D). The proportion of responder (CR/PR) in the LRG was significantly higher than that in the HRG (31% versus 14%) (Figure 7E). Therefore, patients in the LRG may benefit more from immunotherapy than those in the HRG.

We further analyzed RS-related immune activity and evaluated its association with seven clusters (hematopoietic cell kinase [HCK], immunoglobulin G [IgG], interferon, lymphocyte-specific protein tyrosine kinase (LCK), major histocompatibility complex class I [MHC class I], major histocompatibility complex class II [MHC class II], and signal transducer and activator of transcription 1 [STAT1]) representing different inflammatory and immune response functions.[26] High RS was negatively correlated with HCK, LCK, MHC class II, and MHC class I and positively correlated with the interferon cluster (Figure 7F). Due to the close relationship between the seven-gene signature and immune-related biological pathways, we further explored the relationship between risk score and 22 immune cell types. The estimated scores of different immune cell types between the HRG and LRG were calculated via CIBERSORT.

The immune cell landscape differed between the HRG and LRG (Figures 7G, 7H, S2A, and S2B). The abundance of $CD8^+$ cells and M1 macrophages in the LRG was significantly higher than that in the

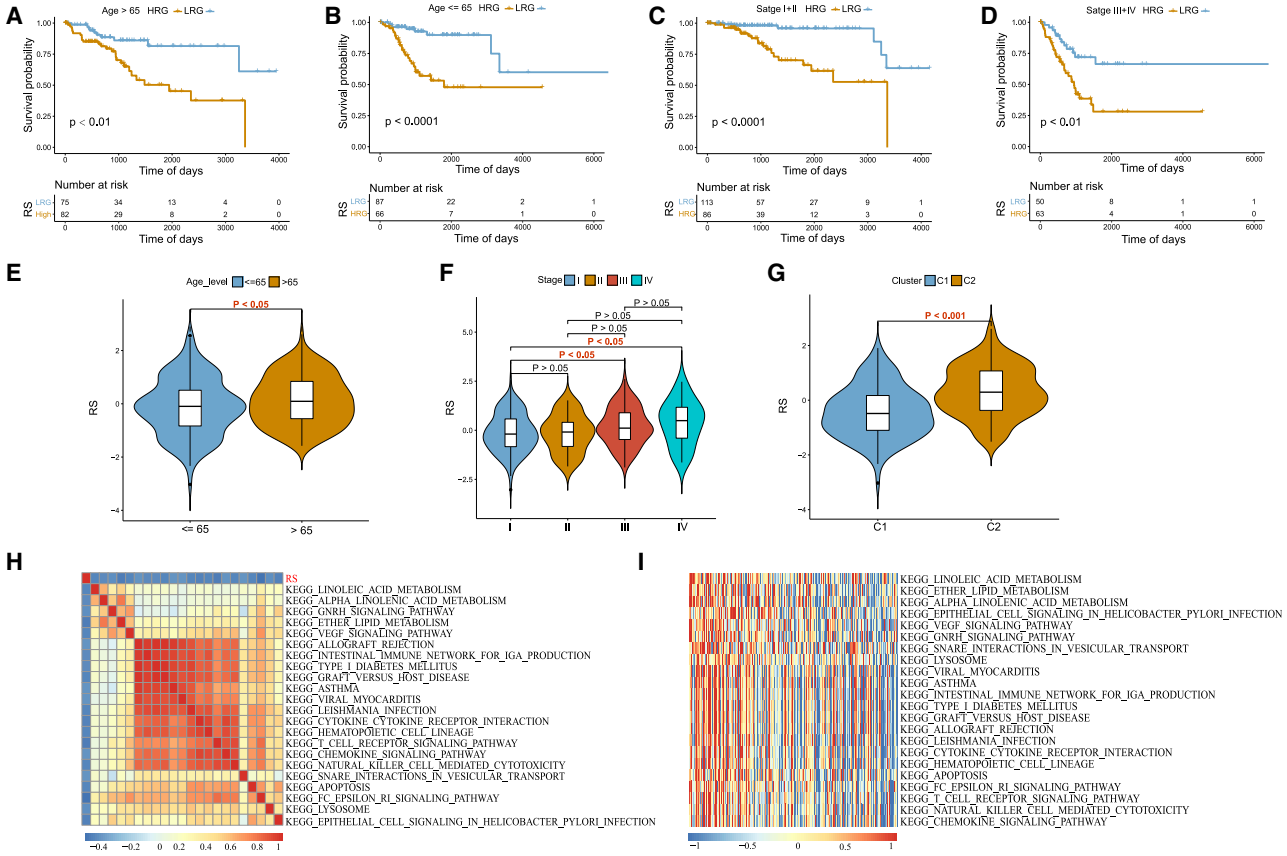

Figure 4. KM survival curves in different clinical subgroups stratified based on the seven-gene risk model

(A) Age >65 years. (B) Age ≤65 years. (C) FIGO stages I + II. (D) FIGO stages III + IV. (E) Correlation diagram between risk score and age. (F) Correlation diagram between risk score and FIGO stage. (G) Correlation diagram between risk score and subtype cluster. (H) The top 22 pathways with RS correlation greater than 0.3. (I) Heatmap of the relationship between pathways and RS; the horizontal axis represents the sample, and the RS increases from left to right.

HRG, suggesting that the TME of HRG was immunosuppressive, which may mechanistically explain the poor prognosis of this patient group.

DISCUSSION

UCEC is a heterogeneous malignancy with distinct molecular characteristics. The prognosis of high-risk endometrial cancer is poor, and the treatment is limited to traditional surgery, radiotherapy, and chemotherapy, the efficacy of which is not satisfactory. Grade III UCEC is a common histological subtype of high-risk endometrial cancer, which makes further exploring its characteristics greatly significant to develop improved clinical diagnosis, treatment, and prognosis approaches. The TIME is instrumental in tumor development and treatment response, especially in immunotherapy. As researchers have shown that numerous immune cells and cytokines are present in endometrial tumors, the anti-tumor immune response may be enhanced via immunotherapy.[27] However, the relationship between patient prognosis and TIME characteristics in endometrial cancer remains poorly understood. The present work focused on grade III endometrial cancer.

A significantly greater abundance of M1 macrophages and $CD8^+$ T cells was observed for C1 than for C2. Activated M1 macrophages suppress tumor growth by releasing pro-inflammatory factors, inducing interstitial damage, and normalizing tumor blood vessels.[28–30] In contrast, M2 tumor-associated macrophages inhibit the anti-tumor immune response by releasing anti-inflammatory cytokines and angiogenic factors. Interestingly, exosomes derived from M1 macrophages repolarize the M2 tumor-associated macrophages into the M1 phenotype, thus enhancing immunotherapy efficacy.[31] Within the tumor immune system, $CD8^+$ T cells are activated by both dendritic cells and costimulatory molecules, which subsequently induces them to attack tumor cells.[32] Blocking the programmed cell death protein 1 (PD-1)-PD-L1 axis can enhance the $CD8^+$ T cell response by preventing $PD\text{-}L1^+$ tumor cell-mediated $CD8^+$ T cell suppression.[33] Thus, we speculated that the C1 subtype may have a better response to immunotherapy.

Based on DEGs between the two subtypes, we constructed a seven-gene signature, composed of DRAM1, TNFRSF14, DNER, SCGB2A1, DAPL1, EMX2, and IFIT1, via Lasso regression. The signature

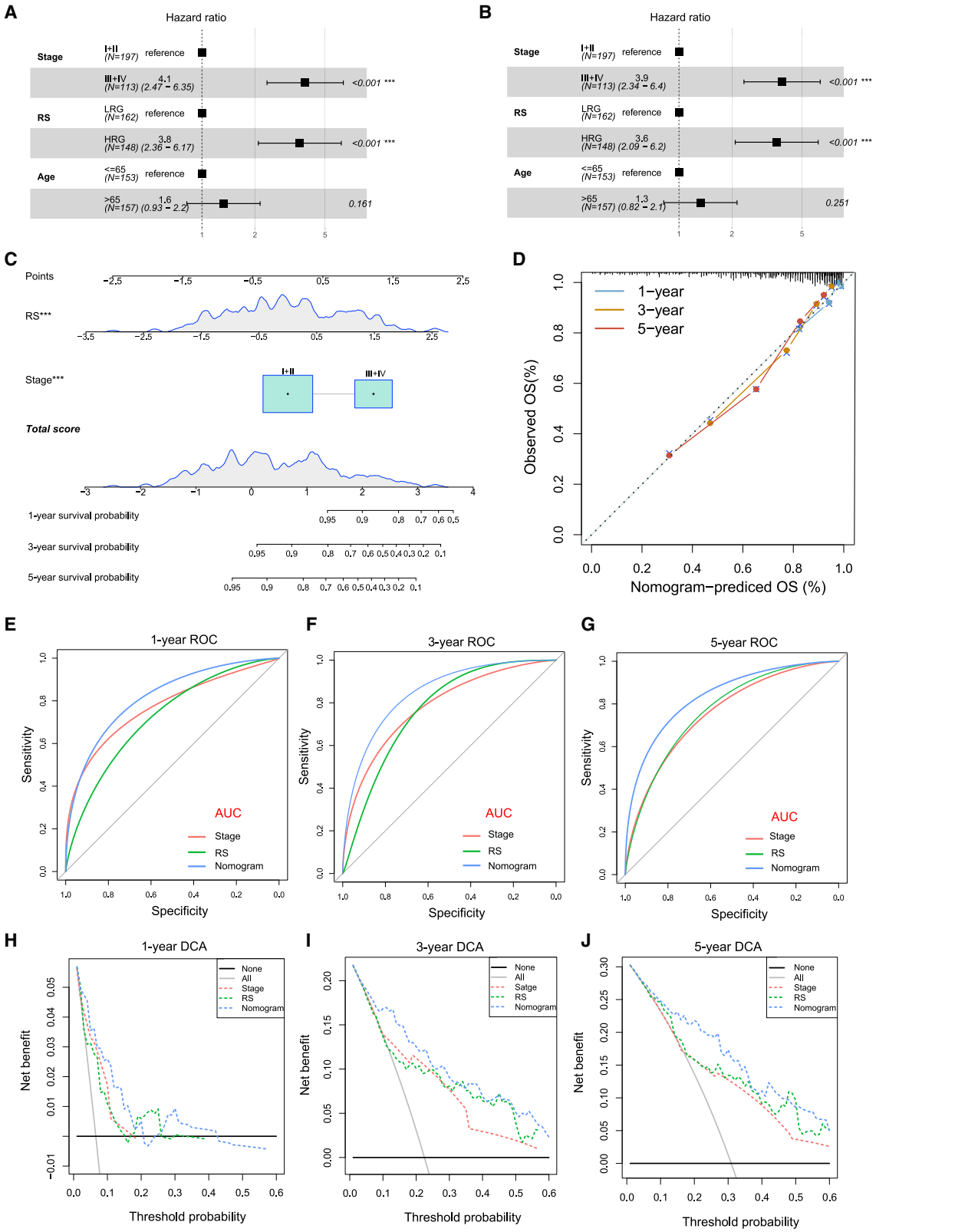

(legend on next page)

robustly predicted prognosis in different datasets. Some studies have shown that SCGB2A1 is overexpressed in endometrial cancer and may be involved in the regulation of tumor proliferation and the cell cycle. Further, the decreased expression of SCGB2A1 was associated with a poor prognosis.[34,35] EMX2 levels in the postmenopausal endometrium were higher than in premenopausal endometrium.[36] Furthermore, EMX2 is significantly downregulated in endometrial cancer.[37] HVEM (TNFRSF14), a member of the TNFR family, is frequently mutated in cancer and is considered to have tumor inhibitory effects in some cancer types. For example, TNFRSF14 may play an anti-tumor role in bladder cancer by inducing cell apoptosis and inhibiting proliferation.[38]

TNFRSF14 acts not only as a ligand of lymphocyte checkpoint proteins BTLA and CD160 but also as a receptor to activate the nuclear factor κB (NF-κB) signaling pathway upon interaction with BTLA and CD160 or TNF ligands LIGHT and LTα, thereby regulating the anti-tumor immune response.[39] IFIT1, which is highly expressed in head and neck squamous cell carcinoma, is associated with several immune checkpoint molecules and tumor-associated macrophage markers.[40] Entestat initiates IFIT1-stimulator of interferon genes (STING)-mediated STAT4 enhancement through interferon regulatory transcription factor 1 (IRF1), thereby enhancing the NK cell-mediated anti-tumor response.[41] Thus, although both TNFRSF14 and IFIT1 are implicated within the TIME, their role in endometrial cancer has not been studied. DRAM1 is a stress-induced regulator of autophagy and cell death associated with cancer, myocardial infarction, and infectious disease.[42] Its acts as a tumor inhibitor in non-small-cell lung carcinoma (NSCLC) by promoting epidermal growth factor receptor (EGFR) lysosome degradation and regulates autophagy as well as cell proliferation by inhibiting the phosphatidylinositol 3-kinase-Akt-mechanistic target of rapamycin (mTOR)-ribosomal protein S6 pathway.[43,44] It has been reported that DNER promotes the epithelial-to-mesenchymal transition in breast cancer through the Wnt/β-catenin pathway.[45] DAPL1 was upregulated in hepatoblastoma and could be used as a prognostic biomarker of the disease.[46] The role of DRAM1, DNER, and DAPL1 in endometrial cancer, as well as their involvement within the immune microenvironment, remains unclear; therefore, further research is needed.

Previous studies have established a prognostic model for UCEC, but they have not specifically targeted grade III high-risk patients with a poor prognosis.[18,21–24,47–49] Among the four prognostic risk models selected for comparison, our model had the highest C-index, indicating that its overall performance was superior. Taken together, our model was a better predictor of patients' outcome.

In clinical practice, the pathologic stage is a key prospective determinant. However, it cannot fully reflect the biological heterogeneity of patients, thus affecting the accuracy of UCEC prediction in patients.

In this study, a seven-gene signature was constructed based on TME-related genes. Moreover, the use of this mRNA-based RS prognostic signature proved to be an effective assessment of patient outcomes. By examining the expression levels of these seven genes, we calculated the RS of each patient: if a patient's RS was greater than 0, this indicates that the patient is at high risk, and his or her prognosis is poor. The clinician may change the patient's treatment plan according to the forecast result of the signature in order to personalize his or her treatment. Additionally, strategies were developed to prevent or detect recurrence of ovarian cancer in high-risk populations as early as possible.

Furthermore, a nomogram comprising FIGO stage and RS was constructed, which allowed us to calculate the level of risk and OS. This approach may contribute to patient counseling and decision-making. In summary, the seven-gene prediction model we constructed will enable ovarian cancer patients to be more accurately managed in clinical practice.

Our model also performed well for predicting the efficacy of immunotherapy. The current findings indicated that risk scores could be used to predict the outcome of anti-PD-L1 therapy in patients with MUC. Furthermore, the combination of RS, NEO, and TMB models could predict treatment responses with an accuracy of 83.3%. Thus, our model may improve immunotherapy treatment choices in G3 endometrial cancer.

RS was also evaluated in relation to tumor immune cell infiltration and inflammation. A high RS was negatively correlated with HCK, LCK, MHC class II, and MHC class I clusters, whereas positively correlated with the interferon cluster. HCK activity is elevated in a variety of malignant solid tumors, promoting the secretion of growth factors and proinflammatory cytokines by myeloid cells as well as the polarization of macrophages to wound healing and alternatively activated phenotypes.[50] LCK, an Src-related protein associated with CD4 and CD8 molecules, is a tyrosine kinase essential for T cell development and activation.[51] Tumors can evade T cell responses by losing the expression of MHC/human leukocyte antigen (HLA) class I.[52] Thus, patients with high RS exhibited an immunosuppressive microenvironment contributing to their relatively poor prognosis. The TME of patients with a low RS was characterized by high infiltration of $CD8^+$ T cells and M1 macrophages.

Figure 5. Clinical value of the predictive model

(A) Forest plot of univariate Cox analysis. (B) Forest plot of multivariate Cox analysis. (C) Nomogram predicting the 1-, 3-, and 5-year OS of patients. The nomogram is applied by adding up the points from the point scale for each variable to a total score. Based the total score, the probability of 1-, 3-, or 5-year survival is projected on the bottom scales. (D) Calibration curves for nomogram-predicted 1-, 3-, and 5-year OS in relation to actual survival. (E–G) ROC curves of nomograms compared with those of other clinical variables with regard to 1-, 3-, and 5-year survival. The DCA curves can evaluate the clinical potential of nomograms. Black indicates that all samples are negative, and none are treated. Therefore, the net benefit is 0. Gray indicates that all samples are positive, and all are treated. The x axis represents threshold probabilities of patients experiencing: (H) 1-year survival; (I) 3-year survival; and (J) 5-year survival.

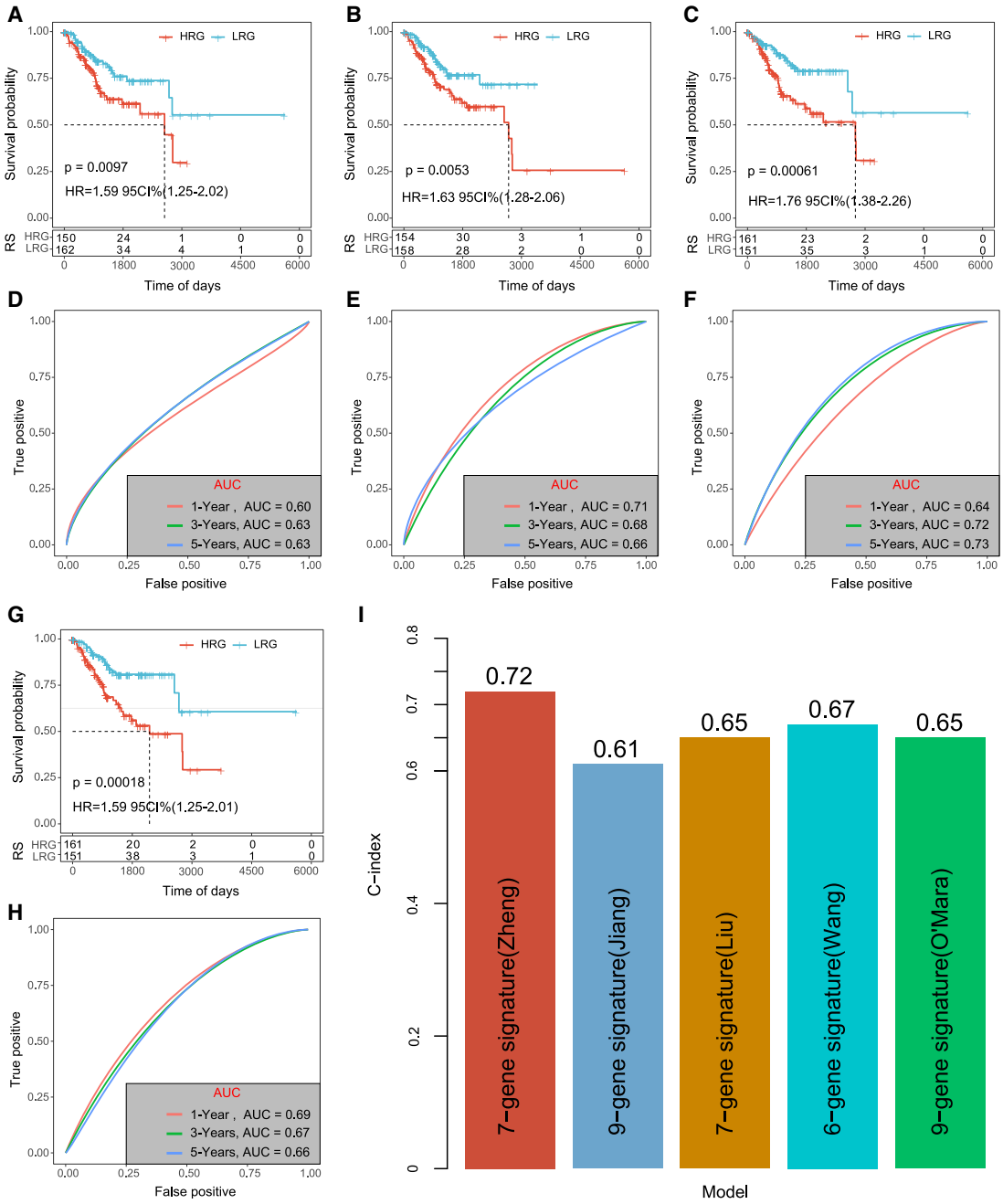

Figure 6. Comparison of the seven-gene risk model with other models

(A and B) The ROC and KM curves of a nine-gene signature (Jiang et al.[21]). (C and D) The ROC and KM curves of another seven-gene signature (Liu et al.[22]). (E and F) The ROC and KM curves of a six-gene signature (Wang et al.[23]). (G and H) The ROC and KM curves of a nine-gene signature (O'Mara et al.[24]). (I) C-indexes of the five risk models.

Studies have shown that OS and disease-free survival are significantly prolonged in patients with UCEC showing high $CD8^+$ T cell tumor infiltration.[53–55] The prognosis of patients with ovarian cancer showing high M1 macrophage infiltration was also favorable.[56–58] Although the relationship between M1 macrophages and endometrial cancer prognosis has been poorly studied, our results suggested that M1 macrophage infiltration may be a predictor of favorable prognosis in grade III UCEC.

The current study does have some limitations. First, we used false discovery rate (FDR) for the multiple hypothesis testing, whereas the Benjamini and Hochberg method was used to calculate FDR. Even

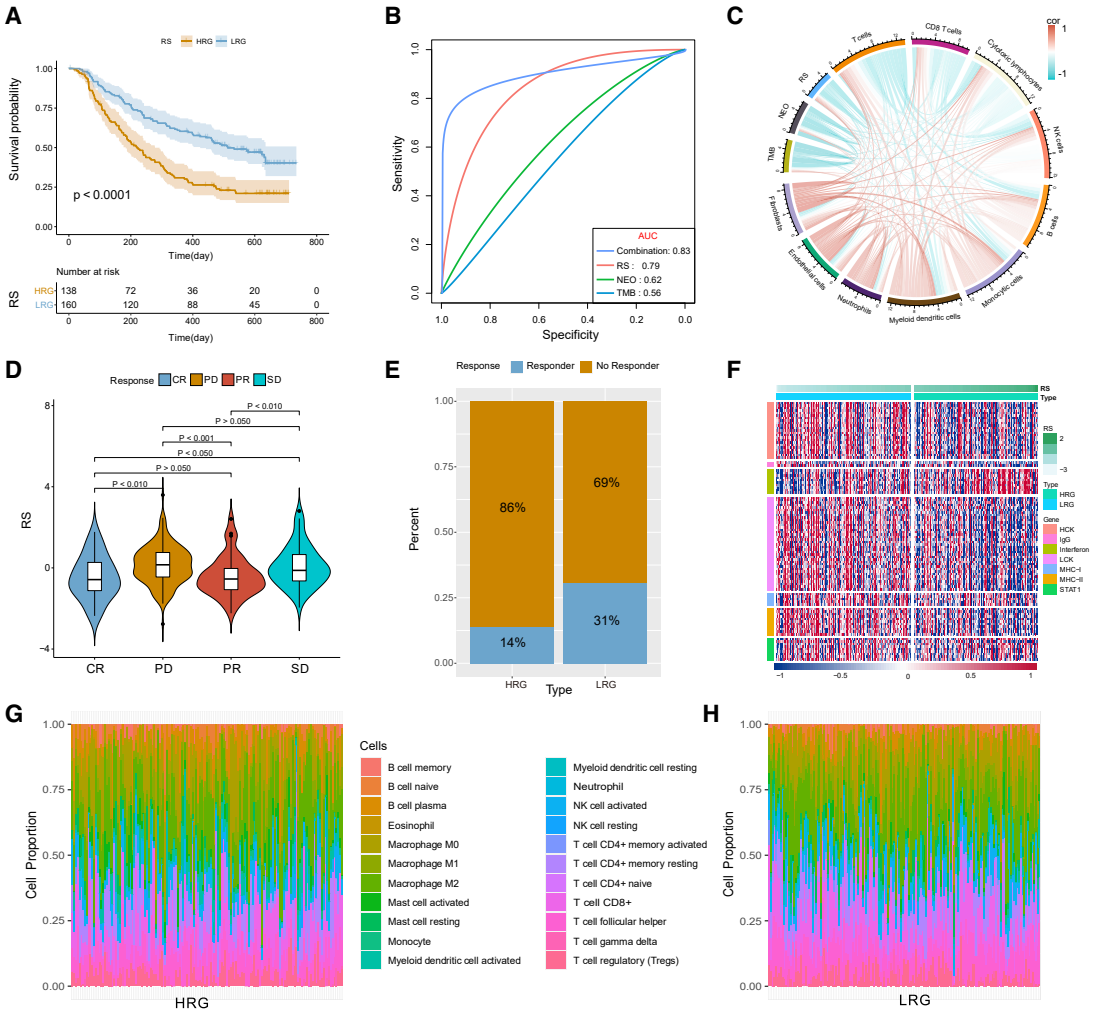

Figure 7. Prediction of immunotherapy response in the IMvigor 210 cohort

(A) The KM curve dividing the cohort in a HRG and a LRG according to the risk score. (B) ROC curve for the prediction of treatment response to PD-L1 blockade comparing TMB, NEO, risk score, and the combination of all three. (C) Correlation among risk score, TMB, NEO, and immune cells. (D) Risk score according to the effectiveness of immunotherapy expressed as CR, PR, SD, or PD. (E) Histogram of the ratio of immunotherapy response between different HRG and LRG in the IMvigor210 cohort. (F) The relationship between risk score and inflammatory activity in patients with G3 UCEC. (G) Distribution of 22 immune cell types in HRG. (H) Distribution of 22 immune cell types in LRG.

though this correction method does not guarantee a complete absence of false positive results, it controls the ratio of false positive results to true positive results within a certain range. Second, at present, the identification of cell types based on RNA sequencing (RNA-seq) depends on the characteristic genes of cells. Hence, different characteristic genes may affect the accuracy of cell-type recognition. Third, due to lack of corresponding clinical samples, we did not have access to an in-house cohort to validate the expression of the seven-gene signature by qRT-PCR or immunochemistry. It is worth noting that some of these genes have not been reported in endometrial cancer and thus remain to be further explored. Finally, TCGA patient population mainly included data from Caucasian and African descendants, which makes the inclusion of Asian populations essential in future research.

In conclusion, we classified high-risk grade III UCEC into C1 and C2 TIME subtypes based on immune-related genes. The C1 subtype may benefit from immunotherapy and also helped elucidate the mechanism underlying this improved response. Thereafter, we constructed and validated a seven-gene prognostic signature, which had good predictive performance in both training and validation cohorts. The RS based on the seven-gene signature could be an important clinical tool for prognosis and for predicting immunotherapy responses in patients with high-risk grade III UCEC.

MATERIALS AND METHODS

Data source and preprocessing

Gene expression profile and clinical follow-up information of RNA-seq samples from patients with UCEC were downloaded from

Table 2. Sample information

Clinical features	TCGA-UCEC	GEO: GSE119041
OS		
0	243	11
1	69	39
Stage		
I	165	
II	34	
III	88	
IV	25	
Age		
≤65	153	
>65	157	
Unknown	2	

TCGA database, and the GEO: GSE 119041 cohort was downloaded from the GEO database.

The RNA-seq data from TCGA-UCEC were preprocessed as follows: (1) the samples without follow-up information were removed; (2) ENSEMBL IDs were converted to gene symbols; (3) grade 3 samples were retained; and (4) genes with expression level lower than 1 and the proportion higher than 50% in all samples were eliminated.

The GEO cohort was processed via the following steps: (1) the samples without clinical follow-up information were removed; (2) ENSEMBL IDs were converted to gene symbols; (3) the probes corresponding to multiple genes were removed; and (4) the median of multiple gene expression values was used.

Data from a total of 312 samples in TCGA-UCEC were collected, and the data for 50 samples were collected from the GEO: GSE119041 cohort. The cohort information is shown in Table 2.

The immune-related pathway genes were downloaded from the website of ImmPort (https://www.immport.org/shared/home) (Table S5).

NMF clustering algorithm

The expression profile of immune-related genes was extracted from TCGA-UCEC cohort, and univariate Cox analysis was performed using the coxph function in R to obtain prognostic genes related ($p < 0.05$). The NMF was used to cluster UCEC samples. A total of 312 grade III UCEC samples were divided into two distinct molecular subtypes with significantly different prognoses (C1 and C2) based on immune prognosis-related genes.

The NMF method selects the standard "Brunet" and performs 100 iterations. The cluster number K was set to 2−10, the average contour width of the common member matrix was determined by the R package "NMF," and the minimum membership of each subclass was set to 10.

Identification of DEGs

The limma R package was used to identify DEGs between the C1 and C2 subtypes by filtering based on the threshold values of FDR < 0.05 and fold change > 1.5. The R software package WebGestaltR (version [v.]0.4.2) was used to conduct Kyoto Encyclopedia of Genes and Genomes (KEGG) pathway and Gene Ontology (GO) functional enrichment analyses of upregulated and downregulated DEGs between UCEC subtypes.

Construction of prognostic risk model

The samples from TCGA dataset were divided into a training and testing cohort. To avoid the influence of random assignment bias on the stability of subsequent modeling, all samples were randomly grouped 100 times in advance. Group sampling was carried out according to a ratio of training cohort: testing cohort equivalent to 1:1. The most suitable training and testing cohorts were selected according to the following conditions: (1) the two groups were similar in age distribution, sex, follow-up time, and patient mortality ratio, and (2) the sample size of the two groups was similar after randomly clustering the gene expression profiling datasets. The chi-square test was used to test both cohorts. No significant differences were observed ($p > 0.05$), indicative of reasonable grouping.

Univariate Cox regression analysis, Lasso regression analysis, and AIC

The univariate Cox proportional hazard regression model was employed using the training set data, and $p < 0.05$ was selected as the filtering threshold. Finally, DEGs from the C1 and C2 subtypes were identified.

The Lasso method is a compression estimate.[59] Since it yields a more refined model by constructing a penalty function, some coefficients are compressed, whereas some coefficients are set to zero. Therefore, it retains the advantage of subset contraction, a kind of biased estimation with complex collinear data, which can realize the selection of variables at the time of parameter estimation, solving the problem of multicollinearity in regression analysis. The DEGs were analyzed by Lasso Cox regression using the R software package glmnet.

AIC was used to conduct stepwise regression, which takes into account the statistical degree of fit of the model and the number of parameters used to fit. The stepAIC method in the MASS package starts with the most complex model and deletes a variable to reduce the AIC. The smaller the value, the better the model, indicating that the model obtains a sufficient degree of fit with fewer parameters. The DEGs were further analyzed by AIC stepwise regression analysis, and the final hub genes were obtained.

Statistical analysis

KM analysis was used to calculate the survival rate, and the log-rank test was used to determine the significance of differences between survival curves. The clinical utility of the prognostic model was evaluated by both time-dependent ROC and DCA analyses. The nomogram was

constructed by integrating the significant clinical features of multivariate Cox analysis using the R package rms, and the pROC package was used to draw the ROC curve. For the IMvigor210 cohort, we used the IMvigor210CoreBiologies package to extract clinical information and gene expression profile information. Afterward, the gene expression profiles were converted from counts to transcripts per million (TPM), and we performed log2 processing. We used the analysis of variance (ANOVA) test to draw a box diagram among CR, PR, SD, and PD. In addition, the Corrplot package was used to plot correlations. All statistical analyses were performed using the R software (v.3.6.1).

SUPPLEMENTAL INFORMATION

Supplemental information can be found online at https://doi.org/10.1016/j.omto.2021.07.002.

ACKNOWLEDGMENTS

The results shown here are in whole or part based upon data generated by TCGA (https://portal.gdc.cancer.gov/), GEO (https://www.ncbi.nlm.nih.gov/geo/), and ImmPort (https://www.immport.org/shared/home). This work was supported by National Natural Science Foundation of China (numbers [nos.] 81672590 and 81472437) and Shengjing Freedom researchers' plan (201804). We acknowledge financial support by the China Scholarship Council for Mingjun Zheng (no. 201908210291).

AUTHOR CONTRIBUTIONS

Conceptualization and methodology, M.Z.; writing – original draft, M.Z. and Y.H.; writing – review & editing, M.Z., Y.H., X.L., and S.L.; validation, M.Z., X.N., and R.G.; project administration and supervision, B.L.

DECLARATION OF INTERESTS

The authors declare no competing interests.

REFERENCES

1. Ferlay, J., Soerjomataram, I., Dikshit, R., Eser, S., Mathers, C., Rebelo, M., Parkin, D.M., Forman, D., and Bray, F. (2015). Cancer incidence and mortality worldwide: sources, methods and major patterns in GLOBOCAN 2012. Int. J. Cancer *136*, E359–E386.
2. Chen, W., Zheng, R., Baade, P.D., Zhang, S., Zeng, H., Bray, F., Jemal, A., Yu, X.Q., and He, J. (2016). Cancer statistics in China, 2015. CA Cancer J. Clin. *66*, 115–132.
3. Ferlay, J., Steliarova-Foucher, E., Lortet-Tieulent, J., Rosso, S., Coebergh, J.W., Comber, H., Forman, D., and Bray, F. (2013). Cancer incidence and mortality patterns in Europe: estimates for 40 countries in 2012. Eur. J. Cancer *49*, 1374–1403.
4. Bendifallah, S., Koskas, M., Ballester, M., Genin, A.-S., Darai, E., and Rouzier, R. (2012). The survival impact of systematic lymphadenectomy in endometrial cancer with the use of propensity score matching analysis. Am. J. Obstet. Gynocol. *206*, 500.e1–500.e11.
5. Creasman, W.T., Odicino, F., Maisonneuve, P., Quinn, M.A., Beller, U., Benedet, J.L., Heintz, A.P., Ngan, H.Y., and Pecorelli, S. (2006). Carcinoma of the corpus uteri. FIGO 26th Annual Report on the Results of Treatment in Gynecological Cancer. Int. J. Gynaecol. Obstet. *95* (*Suppl 1*), S105–S143.
6. Nugent, E.K., Bishop, E.A., Mathews, C.A., Moxley, K.M., Tenney, M., Mannel, R.S., Walker, J.L., Moore, K.N., Landrum, L.M., and McMeekin, D.S. (2012). Do uterine risk factors or lymph node metastasis more significantly affect recurrence in patients with endometrioid adenocarcinoma? Gynecol. Oncol. *125*, 94–98.
7. Bendifallah, S., Canlorbe, G., Raimond, E., Hudry, D., Coutant, C., Graesslin, O., Touboul, C., Huguet, F., Cortez, A., Daraï, E., and Ballester, M. (2014). A clue towards improving the European Society of Medical Oncology risk group classification in apparent early stage endometrial cancer? Impact of lymphovascular space invasion. Br. J. Cancer *110*, 2640–2646.
8. Bendifallah, S., Canlorbe, G., Collinet, P., Arsène, E., Huguet, F., Coutant, C., Hudry, D., Graesslin, O., Raimond, E., Touboul, C., et al. (2015). Just how accurate are the major risk stratification systems for early-stage endometrial cancer? Br. J. Cancer *112*, 793–801.
9. Moore, K.N., and Fader, A.N. (2011). Uterine papillary serous carcinoma. Clin. Obstet. Gynecol. *54*, 278–291.
10. Xiao, Y., and Yu, D. (2021). Tumor microenvironment as a therapeutic target in cancer. Pharmacol. Ther. *221*, 107753.
11. Ren, B., Cui, M., Yang, G., Wang, H., Feng, M., You, L., and Zhao, Y. (2018). Tumor microenvironment participates in metastasis of pancreatic cancer. Mol. Cancer *17*, 108.
12. Luo, Z., Wang, Q., Lau, W.B., Lau, B., Xu, L., Zhao, L., Yang, H., Feng, M., Xuan, Y., Yang, Y., et al. (2016). Tumor microenvironment: The culprit for ovarian cancer metastasis? Cancer Lett. *377*, 174–182.
13. Jiang, Y., Wang, C., and Zhou, S. (2020). Targeting tumor microenvironment in ovarian cancer: Premise and promise. Biochim. Biophys. Acta Rev. Cancer *1873*, 188361.
14. Yang, L., and Lin, P.C. (2017). Mechanisms that drive inflammatory tumor microenvironment, tumor heterogeneity, and metastatic progression. Semin. Cancer Biol. *47*, 185–195.
15. Degos, C., Heinemann, M., Barrou, J., Boucherit, N., Lambaudie, E., Savina, A., Gorvel, L., and Olive, D. (2019). Endometrial Tumor Microenvironment Alters Human NK Cell Recruitment, and Resident NK Cell Phenotype and Function. Front. Immunol. *10*, 877.
16. Wang, Z., Gerstein, M., and Snyder, M. (2009). RNA-Seq: a revolutionary tool for transcriptomics. Nat. Rev. Genet. *10*, 57–63.
17. Wang, X., Dai, C., Ye, M., Wang, J., Lin, W., and Li, R. (2021). Prognostic value of an autophagy-related long-noncoding-RNA signature for endometrial cancer. Aging (Albany NY) *13*, 5104–5119.
18. Jiang, Y., Chen, J., Ling, J., Zhu, X., Jiang, P., Tang, X., Zhou, H., and Li, R. (2021). Construction of a Glycolysis-related long noncoding RNA signature for predicting survival in endometrial cancer. J. Cancer *12*, 1431–1444.
19. Liu, J., Li, S., Feng, G., Meng, H., Nie, S., Sun, R., Yang, J., and Cheng, W. (2020). Nine glycolysis-related gene signature predicting the survival of patients with endometrial adenocarcinoma. Cancer Cell Int. *20*, 183.
20. Zhou, M., Zhang, Z., Zhao, H., Bao, S., and Sun, J. (2018). A novel lncRNA-focus expression signature for survival prediction in endometrial carcinoma. BMC Cancer *18*, 39.
21. Jiang, P., Sun, W., Shen, N., Huang, X., and Fu, S. (2020). Identification of a metabolism-related gene expression prognostic model in endometrial carcinoma patients. BMC Cancer *20*, 864.
22. Liu, L., Lin, J., and He, H. (2019). Identification of Potential Crucial Genes Associated With the Pathogenesis and Prognosis of Endometrial Cancer. Front. Genet. *10*, 373.
23. Wang, Y., Ren, F., Chen, P., Liu, S., Song, Z., and Ma, X. (2018). Identification of a six-gene signature with prognostic value for patients with endometrial carcinoma. Cancer Med. *7*, 5632–5642.
24. O'Mara, T.A., Zhao, M., and Spurdle, A.B. (2016). Meta-analysis of gene expression studies in endometrial cancer identifies gene expression profiles associated with aggressive disease and patient outcome. Sci. Rep. *6*, 36677.
25. Rosenberg, J.E., Hoffman-Censits, J., Powles, T., van der Heijden, M.S., Balar, A.V., Necchi, A., Dawson, N., O'Donnell, P.H., Balmanoukian, A., Loriot, Y., et al. (2016). Atezolizumab in patients with locally advanced and metastatic urothelial carcinoma who have progressed following treatment with platinum-based chemotherapy: a single-arm, multicentre, phase 2 trial. Lancet *387*, 1909–1920.
26. Huang, E., Cheng, S.H., Dressman, H., Pittman, J., Tsou, M.H., Horng, C.F., Bild, A., Iversen, E.S., Liao, M., Chen, C.M., et al. (2003). Gene expression predictors of breast cancer outcomes. Lancet *361*, 1590–1596.

27. Rodriguez-Garcia, A., Minutolo, N.G., Robinson, J.M., and Powell, D.J. (2017). T-cell target antigens across major gynecologic cancers. Gynecol. Oncol. *145*, 426–435.

28. Chanmee, T., Ontong, P., Konno, K., and Itano, N. (2014). Tumor-associated macrophages as major players in the tumor microenvironment. Cancers (Basel) *6*, 1670–1690.

29. Mills, C.D., Lenz, L.L., and Harris, R.A. (2016). A Breakthrough: Macrophage-Directed Cancer Immunotherapy. Cancer Res. *76*, 513–516.

30. Hanahan, D., and Coussens, L.M. (2012). Accessories to the crime: functions of cells recruited to the tumor microenvironment. Cancer Cell *21*, 309–322.

31. Choo, Y.W., Kang, M., Kim, H.Y., Han, J., Kang, S., Lee, J.R., Jeong, G.J., Kwon, S.P., Song, S.Y., Go, S., et al. (2018). M1 Macrophage-Derived Nanovesicles Potentiate the Anticancer Efficacy of Immune Checkpoint Inhibitors. ACS Nano *12*, 8977–8993.

32. Diamond, M.S., Kinder, M., Matsushita, H., Mashayekhi, M., Dunn, G.P., Archambault, J.M., Lee, H., Arthur, C.D., White, J.M., Kalinke, U., et al. (2011). Type I interferon is selectively required by dendritic cells for immune rejection of tumors. J. Exp. Med. *208*, 1989–2003.

33. Kamphorst, A.O., Wieland, A., Nasti, T., Yang, S., Zhang, R., Barber, D.L., Konieczny, B.T., Daugherty, C.Z., Koenig, L., Yu, K., et al. (2017). Rescue of exhausted CD8 T cells by PD-1-targeted therapies is CD28-dependent. Science *355*, 1423–1427.

34. Zhou, H., Zou, X., Li, H., Li, T., Chen, L., and Cheng, X. (2020). Decreased secretoglobin family 2A member 1expression is associated with poor outcomes in endometrial cancer. Oncol. Lett. *20*, 24.

35. Dieters-Castator, D.Z., Rambau, P.F., Kelemen, L.E., Siegers, G.M., Lajoie, G.A., Postovit, L.M., and Köbel, M. (2019). Proteomics-Derived Biomarker Panel Improves Diagnostic Precision to Classify Endometrioid and High-grade Serous Ovarian Carcinoma. Clin. Cancer Res. *25*, 4309–4319.

36. Noonan, F.C., Mutch, D.G., Ann Mallon, M., and Goodfellow, P.J. (2001). Characterization of the homeodomain gene EMX2: sequence conservation, expression analysis, and a search for mutations in endometrial cancers. Genomics *76*, 37–44.

37. Qiu, H., Yan, Q., Luo, X., Zhang, H., Bao, W., and Wan, X. (2013). EMX2 is downregulated in endometrial cancer and correlated with tumor progression. Int. J. Gynecol. Pathol. *32*, 193–198.

38. Zhu, Y.D., and Lu, M.Y. (2018). Increased expression of TNFRSF14 indicates good prognosis and inhibits bladder cancer proliferation by promoting apoptosis. Mol. Med. Rep. *18*, 3403–3410.

39. Šedý, J.R., and Ramezani-Rad, P. (2019). HVEM network signaling in cancer. Adv. Cancer Res. *142*, 145–186.

40. Li, H., Yang, L.L., Wu, C.C., Xiao, Y., Mao, L., Chen, L., Zhang, W.F., and Sun, Z.J. (2020). Expression and Prognostic Value of IFIT1 and IFITM3 in Head and Neck Squamous Cell Carcinoma. Am. J. Clin. Pathol. *153*, 618–629.

41. Idso, J.M., Lao, S., Schloemer, N.J., Knipstein, J., Burns, R., Thakar, M.S., and Malarkannan, S. (2020). Entinostat augments NK cell functions via epigenetic upregulation of IFIT1-STING-STAT4 pathway. Oncotarget *11*, 1799–1815.

42. Zhang, R., Varela, M., Forn-Cuní, G., Torraca, V., van der Vaart, M., and Meijer, A.H. (2020). Deficiency in the autophagy modulator Dram1 exacerbates pyroptotic cell death of Mycobacteria-infected macrophages. Cell Death Dis. *11*, 277.

43. Geng, J., Zhang, R., Yuan, X., Xu, H., Zhu, Z., Wang, X., Wang, Y., Xu, G., Guo, W., Wu, J., and Qin, Z.H. (2020). DRAM1 plays a tumor suppressor role in NSCLC cells by promoting lysosomal degradation of EGFR. Cell Death Dis. *11*, 768.

44. Lu, T., Zhu, Z., Wu, J., She, H., Han, R., Xu, H., and Qin, Z.H. (2019). DRAM1 regulates autophagy and cell proliferation via inhibition of the phosphoinositide 3-kinase-Akt-mTOR-ribosomal protein S6 pathway. Cell Commun. Signal. *17*, 28.

45. Wang, Z., Li, Z., Wu, Q., Li, C., Li, J., Zhang, Y., Wang, C., Sun, S., and Sun, S. (2020). DNER promotes epithelial-mesenchymal transition and prevents chemosensitivity through the Wnt/β-catenin pathway in breast cancer. Cell Death Dis. *11*, 642.

46. Rodrigues, T.C., Fidalgo, F., da Costa, C.M., Ferreira, E.N., da Cunha, I.W., Carraro, D.M., Krepischi, A.C., and Rosenberg, C. (2014). Upregulated genes at 2q24 gains as candidate oncogenes in hepatoblastomas. Future Oncol. *10*, 2449–2457.

47. Deng, F., Mu, J., Qu, C., Yang, F., Liu, X., Zeng, X., and Peng, X. (2021). A Novel Prognostic Model of Endometrial Carcinoma Based on Clinical Variables and Oncogenomic Gene Signature. Front. Mol. Biosci. *7*, 587822.

48. Liu, J., Jiang, P., Chen, X., Shen, Y., Cui, G., Ma, Z., Zhao, S., and Zhang, Y. (2021). Construction of a nine DNA repair-related gene prognostic classifier to predict prognosis in patients with endometrial carcinoma. BMC Cancer *21*, 29.

49. Li, X., Yin, F., Fan, Y., Cheng, Y., Dong, Y., Zhou, J., Wang, Z., Li, X., and Wang, J. (2021). Establishment and validation of a prognostic nomogram based on a novel five-DNA methylation signature for survival in endometrial cancer patients. Cancer Med. *10*, 693–708.

50. Poh, A.R., O'Donoghue, R.J., and Ernst, M. (2015). Hematopoietic cell kinase (HCK) as a therapeutic target in immune and cancer cells. Oncotarget *6*, 15752–15771.

51. Salmond, R.J., Filby, A., Qureshi, I., Caserta, S., and Zamoyska, R. (2009). T-cell receptor proximal signaling via the Src-family kinases, Lck and Fyn, influences T-cell activation, differentiation, and tolerance. Immunol. Rev. *228*, 9–22.

52. Garrido, F., and Aptsiauri, N. (2019). Cancer immune escape: MHC expression in primary tumours versus metastases. Immunology *158*, 255–266.

53. Guo, F., Dong, Y., Tan, Q., Kong, J., and Yu, B. (2020). Tissue Infiltrating Immune Cells as Prognostic Biomarkers in Endometrial Cancer: A Meta-Analysis. Dis. Markers *2020*, 1805764.

54. de Jong, R.A., Leffers, N., Boezen, H.M., ten Hoor, K.A., van der Zee, A.G., Hollema, H., and Nijman, H.W. (2009). Presence of tumor-infiltrating lymphocytes is an independent prognostic factor in type I and II endometrial cancer. Gynecol. Oncol. *114*, 105–110.

55. Kondratiev, S., Sabo, E., Yakirevich, E., Lavie, O., and Resnick, M.B. (2004). Intratumoral CD8+ T lymphocytes as a prognostic factor of survival in endometrial carcinoma. Clin. Cancer Res. *10*, 4450–4456.

56. Macciò, A., Gramignano, G., Cherchi, M.C., Tanca, L., Melis, L., and Madeddu, C. (2020). Role of M1-polarized tumor-associated macrophages in the prognosis of advanced ovarian cancer patients. Sci. Rep. *10*, 6096.

57. Zhang, M., He, Y., Sun, X., Li, Q., Wang, W., Zhao, A., and Di, W. (2014). A high M1/M2 ratio of tumor-associated macrophages is associated with extended survival in ovarian cancer patients. J. Ovarian Res. *7*, 19.

58. Reinartz, S., Schumann, T., Finkernagel, F., Wortmann, A., Jansen, J.M., Meissner, W., Krause, M., Schwörer, A.M., Wagner, U., Müller-Brüsselbach, S., and Müller, R. (2014). Mixed-polarization phenotype of ascites-associated macrophages in human ovarian carcinoma: correlation of CD163 expression, cytokine levels and early relapse. Int. J. Cancer *134*, 32–42.

59. Tibshirani, R. (1996). Regression shrinkage and selection via the lasso: a retrospective. J. R. Stat. Soc. Series B Stat. Methodol. *58*, 267–288.